Journal of *Marine Science and Engineering*

MDPI

Article

Numerical Study and Geometrical Investigation of an Onshore Overtopping Device Wave Energy Converter with a Seabed Coupled Structure

Andréia S. de Barros [1], Cristiano Fragassa [2,*], Maycon da S. Paiva [3], Luiz A. O. Rocha [1], Bianca N. Machado [4], Liércio A. Isoldi [1], Mateus das N. Gomes [5] and Elizaldo D. dos Santos [1]

1 School of Engineering, Federal University of Rio Grande (FURG), Italia Av., Km 8, Rio Grande 96203-900, RS, Brazil
2 Department of Industrial Engineering, University of Bologna, Viale Risorgimento 2, 40136 Bologna, Italy
3 Department of Pure and Applied Mathematics, Federal University of Rio Grande do Sul, Bento Gonçalves Av., 9500, Porto Alegre 91509-900, RS, Brazil
4 Interdisciplinary Department, Federal University of Rio Grande do Sul (UFRGS), RS 030, 11.700-Km 92 Emboaba, Tramandaí 95590-000, RS, Brazil
5 Federal Institute of Paraná (IFPR), Antônio Carlos Rodrigues Av., 453, Paranaguá 83215-750, PR, Brazil
* Correspondence: cristiano.fragassa@unibo.it; Tel.: +39-347-697-4046

Abstract: Studies regarding renewable energy sources have gained attention over recent years. One example is wave energy converters, which harvest energy from sea waves using different operational principles such as oscillating water columns, oscillating bodies, and overtopping devices. In the present paper, a numerical study is carried out, and a geometrical investigation of a full-scale overtopping device with a coupled structure mounted on the seabed is performed using the Constructal Design method. The main purpose is to investigate the influence of the design over the available power of the device. The areas of the overtopping ramp (A_r) and the trapezoidal seabed structure (A_t) are the problem constraints. Two degrees of freedom are studied, the ratio between the height and length of the ramp (H_3/L_3) and the ratio between the upper and lower basis of the trapezoidal obstacle (L_1/L_2). The device submersion is kept constant (H_1 = 3.5 m). The equations of continuity, momentum, and the transport of volume fraction are solved with the Finite Volume Method, while the water–air mixture is treated with the multiphase model Volume of Fluid. Results showed that the ratio H_3/L_3 presented a higher sensibility than the ratio L_1/L_2 over the accumulated water in the reservoir. Despite that, the association of a structure coupled to the ramp of an overtopping device improved the performance of the converter by 30% compared to a conventional condition without the structure.

Keywords: numerical simulation; geometric analysis; overtopping device; seabed structure; constructal design

Citation: de Barros, A.S.; Fragassa, C.; Paiva, M.d.S.; Rocha, L.A.O.; Machado, B.N.; Isoldi, L.A.; Gomes, M.d.N.; dos Santos, E.D. Numerical Study and Geometrical Investigation of an Onshore Overtopping Device Wave Energy Converter with a Seabed Coupled Structure. *J. Mar. Sci. Eng.* **2023**, *11*, 412. https://doi.org/10.3390/jmse11020412

Received: 21 January 2023
Revised: 6 February 2023
Accepted: 8 February 2023
Published: 13 February 2023

1. Introduction

The use of renewable energy sources has become necessary due to the increase in energy demand and environmental problems caused by the consumption of fossil fuels [1]. Thereby, Hernández-Fontes [2] highlights ocean energy resources as an alternative way to supply energy with several magnitudes. However, various difficulties have been faced in exploring the potential energy on a large scale, challenging the consolidation of wave energy converters in the commercial form [3].

Despite the adverse sea conditions regarding the installation and maintenance of wave energy converters (WECs), many experimental studies have indicated that devices with different physical operating principles can harvest energy from sea waves [4–11]. According to Pecher and Kofoed [12], different WECs can be classified according to the

following main operational principles: oscillating water column (OWC), with fixed or floating structure; oscillating, floating, or submerged bodies; and overtopping, with a fixed or floating structure. However, there are WECs where the physical operating principles do not fit into the mentioned classification, e.g., the Submerged Horizontal Plate [13–15].

The present object of study is an onshore overtopping WEC. This device is accessible by land, which guarantees greater practicality in installation and maintenance. The operating principle of the device consists of guiding sea waves through a ramp to a reservoir located above mean sea level, transforming kinetic energy into potential energy. The water accumulated in the reservoir returns to the sea flowing through a low-head turbine, generating electricity [12,16].

Over the last few years, overtopping devices and breakwaters have been investigated by means of experimental and numerical works [4–7,9,17–20]. Recent developments have been achieved related to the comprehension of the influence of multiple ramps and stages of reservoirs in overtopping devices [5], investigation of hybrid converters associating the overtopping device in a harbor breakwater with an oscillating water column device [6], and integration of overtopping devices with breakwater structures [17,18]. In the latter subject, Han et al. [17] numerically evaluated the performance of multi-level overtopping breakwater for energy conversion (MOBREC). The device was composed of two reservoirs with sloping walls at different levels. More precisely, the effect of parameters such as angles of the ramps, the width of the opening of the lower reservoir, and the height of the space between the reservoirs over the dimensionless discharge of water of the device was investigated. Afterward, Lauro et al. [18] analyzed the hydraulic performance and stability of a vertical breakwater with an overtopping device attached to its top. The device was named OBREC-V and consisted of a concrete structure with a frontal ramp capable of capturing and collecting part of the incident wave energy. Simulations were carried out to compare the performance of the structure under the action of irregular waves in terms of wave reflection, overtopping, and wave acting forces. Results indicated a reduction in destabilizing forces acting in the breakwater compared to a traditional structure. Recently, the OBREC device was investigated and installed for field tests, obtaining important recommendations about the design under sea conditions [19,20]. In the work of Contestabile et al. [19], for example, the effect of a structure coupled to the reservoir of overtopping (parapet) to improve the protection of the coast and, at the same time, to augment the wave energy conversion was investigated. Some tests were performed considering the influence of the geometry of the parapet for different water levels. Later, Contestabile et al. [20] investigated the effects of sea winds and land breeze circulations for wind and wave energy conversion on the Gulf of Naples (Italy) coast, considering a dataset of 42 years. A case study was analyzed at the Marine Renewable Energy Laboratory and generated recommendations about exploring multivariable techniques such as wind and wave technologies for wave energy conversion. For the coast conditions studied, results indicated that the production would be more available and less variable when the combined wave-wind farm is installed.

One important aspect of defining the overtopping devices lies in the investigation of the influence of the design on the performance of the WECs. Recently, Constructal theory [21] has been used to obtain recommendations about the geometry of WECs [22–27]. Constructal theory is the view that the design of any finite-size flow system is ruled by a physical principle, including what is seen in nature [21,28]. The physical principle that leads to the formation of these flow systems is called the Constructal Law, which states that for a given finite-size flow system to persist in time, its design must freely evolve in such a way that it provides easier access to the imposed currents that flow through it [29–31]. Constructal Design [21,31] is the method used to investigate the influence of the design of a finite-size flow system over its performance. In this method, the geometry is deduced from a principle of increase in performance while the system is subjected to constraints and varied according to the defined degrees of freedom.

Concerning the application of Constructal Design on overtopping devices, Dos Santos et al. [22] performed a geometric study of an offshore device at a laboratory scale. More

precisely, the influence of the height/length ratio of the ramp for different relative depths (given by the ratio between the depth of the wave channel and the length of the monochromatic wave used) on the accumulated water into the device reservoir was evaluated. Later, Goulart et al. [23] evaluated the influence of a ramp geometry on the performance of a full-scale onshore overtopping device under the incidence of regular waves. The ratio between the height and length of the ramp that maximizes the mass of water accumulated in the reservoir for distances of 5.0 m and 6.0 m between the bottom of the device and the bottom of the channel was investigated. Martins et al. [24] evaluated the effect of the slope of the ramp and the submersion of the device on the available power of a full-scale onshore overtopping device, considering three different areas for the ramp, as well as the incidence of two different monochromatic waves. Recently, Martins et al. [22] carried out a numerical study on an overtopping device with one and two ramps incorporated into a breakwater placed on the south coast of Brazil, which has a high potential for conversion of wave energy [32,33], and subjected to irregular waves modeled with the JONSWAP spectrum. The authors identified that, for future studies, the use of a realistic database could contribute even more to predicting the design of overtopping devices under more realistic conditions. Progress has been made towards this kind of prediction, as seen in the recent methodology named WaveMIMO [34–36]. It is also important to mention that an overtopping device can be used in coastal placements for two purposes, coastal defense and wave energy conversion. Moreover, recent works have demonstrated that increasing renewable energy availability is one of the main challenges. In this sense, the study of wind-wave energy in combination has been indicated as a future strategy for energy conversion [20]. Recently, new contributions have been proposed to use new strategies for power take-off, such as triboelectric nanogenerators for energy conversion [37]. For example, Jiao et al. [37] developed numerical and experimental investigations on magnetic capsulate triboelectric nanogenerators. The authors observed that the proposed device provided an effective form to harvest electrical energy from low-frequency and low-amplitude oscillations, which is adequate for converting wave energy. Another strategy for future devices is the improvement of design in order to increase wave energy conversion efficiency, being the contribution proposed here for overtopping devices.

Despite the numerous works found in the literature, none of these studies investigated the effect that the geometry of obstacles positioned on the seabed has on the amount of water accumulated in the reservoir of an overtopping device where the obstacle is coupled. Thereby, the present paper aims to evaluate the geometry of a trapezoidal obstacle at the bottom of a full-scale wave channel coupled with an onshore overtopping device, being the main contribution to the detailed investigation of the geometric configuration of the device performance. The geometry is investigated using the Constructal Design method, and the geometrical optimization is performed with exhaustive search, allowing the comprehension of the effect of degrees of freedom of the problem over the performance indicator (water accumulated in the reservoir). To the best of the authors' knowledge, this kind of investigation was not previously performed in the literature.

2. Mathematical Modeling

The Volume of Fluid (VOF) multiphase model [38] was employed, which makes it possible to represent two or more immiscible fluids by solving a transport equation for volume fraction along the domain. In each control volume, the sum of the volume fraction of all phases is unity. Therefore, once there are two different phases, air and water, the concept of volume fraction (α) is used to represent the two phases within a control volume. Thus, 0 indicates that the control volume does not contain one of the phases (α_{water} or α_{air}), while 1 indicates that only this phase is contained in the volume. If the volume contains a mixture of air and water, then:

$$\alpha_{air} = 1 - \alpha_{water} \quad (1)$$

According to Schlichting [39], the mass conservation equation for a mixture of air and water in an isothermal, laminar, and incompressible flow is given by:

$$\frac{\partial \rho}{\partial t} + \nabla \cdot \left(\rho \vec{v} \right) = 0 \tag{2}$$

where ρ is the fluid density (kg/m^3); t is the time (s); $\vec{v}$ is the velocity vector (m/s). The momentum equation for the mixture is given by:

$$\frac{\partial \rho \vec{v}}{\partial t} + \nabla \cdot \left(\rho \vec{v} \vec{v} \right) = -\nabla p + \nabla \cdot \left(\mu \overline{\overline{\tau}} \right) + \rho \vec{g} \tag{3}$$

where p is the static pressure (Pa); μ is the dynamic viscosity (kg/(m.s)); $\vec{g}$ is the gravity acceleration vector (m/s^2); and $\overline{\overline{\tau}}$ is the strain rate tensor (N/m^2), which for a Newtonian fluid, is represented by:

$$\overline{\overline{\tau}} = \mu \left(\nabla \cdot \vec{v} + \nabla \cdot \vec{v}^{T} \right) \tag{4}$$

Finally, the volume fraction transport equation is given by [38]:

$$\frac{\partial \alpha_{water}}{\partial t} + \nabla \cdot \left(\alpha_{water} \vec{v} \right) = 0 \tag{5}$$

Since the conservation mass and momentum equations are solved for the mixture, it is necessary to obtain the specific mass and viscosity values for the mixture, which can be written by:

$$\rho = \alpha_{water} \rho_{water} + (1 - \alpha_{water}) \rho_{air} \tag{6}$$

$$\mu = \alpha_{water} \mu_{water} + (1 - \alpha_{water}) \mu_{air} \tag{7}$$

2.1. Wave Generation

Regarding the numerical wave generation, a velocity profile is imposed on the left wall of the channel, simulating the behavior of a wave generator, similar to that performed in previous works [13,18,24]. Table 1 presents the characteristics adopted for the regular waves considered in this study.

Table 1. Characteristics of the regular waves.

Characteristic	Nomenclature	Magnitude
Wave height	H (m)	1.00
Wave period	T (s)	7.50
Wavelength	λ (m)	64.50
Water depth	h (m)	10.00

According to Chakrabarti [40], these waves correspond to the second-order Stokes theory. Therefore, the velocity potential and the free surface elevation of the water can be described, respectively, by [40,41]:

$$\varphi = \frac{gH}{2kc} \frac{\cosh[k(z+k)]}{\cosh(kh)} \sin(kx - \omega t) + \frac{3}{32} ckH^2 \frac{\cosh[2k(z+h)]}{\sinh^4(kh)} \sin[2(kx - \omega t)] \tag{8}$$

$$\eta = \frac{H}{2} \cos(kx - \omega t) + \frac{kH^2}{16} \frac{\cosh(kh)}{\sinh^3(kh)} [2 + \cosh(2kh)] \cos[2(kx - \omega t)] \tag{9}$$

φ being the velocity potential (m^2/s); η the water-free surface elevation (m); x and z, respectively, the horizontal and vertical coordinate axis (m); c the wave celerity (m/s); k the

wave number (m^{-1}); and ω the angular frequency (Hz). Furthermore, the wave number and angular frequency are given, respectively, by:

$$c = \frac{\lambda}{T} = \sqrt{\frac{g}{k}\tanh(kh)} \tag{10}$$

$$k = \frac{2\pi}{\lambda} \tag{11}$$

$$\omega = \frac{2\pi}{T} \tag{12}$$

Thus, by deriving the velocity potential equation for each coordinate axis, it is possible to analytically determine the velocity components given, respectively, by [40,41]:

$$u = \frac{gH}{2c}\frac{\cosh[k(z+h)]}{\cosh(kh)}\cos(kx-\omega t) + \frac{3}{16}ck^2H^2\frac{\cosh[2k(z+h)]}{\sin^4(kh)}\cos[2(kx-\omega t)] \tag{13}$$

$$w = \frac{gH}{2c}\frac{\sinh[k(z+h)]}{\cosh(kh)}\sin(kx-\omega t) + \frac{3}{16}ck^2H^2\frac{\sinh[2k(z+h)]}{\sinh^4(kh)}\sin[2(kx-\omega t)] \tag{14}$$

where u is the horizontal velocity component (m/s); w is the vertical velocity component (m/s).

Aiming to verify the numerical model employed, the free surface elevation of the water on the wave channel was monitored through a gauge located at $x = 50.00$ m. The numerical data obtained were then compared to the analytical results given by Equation (9) using the mean absolute error, given by [42]:

$$MAE = \frac{\sum_{i=1}^{N}|O_i - P_i|}{N} \tag{15}$$

where O_i represents the numerical value (m); P_i is the analytical value (m); and N represents the total number of data, i.e., the number of time steps.

2.2. Problem Description and Geometrical Investigation

The physical problem consists of a wave channel with a trapezoidal obstacle coupled to an overtopping device placed at the bottom of the channel, as can be observed in Figure 1. Therefore, a two-dimensional numerical model was considered, as in [13,22–27,34–36], because this simplification adequately represented the incidence of waves and led to a significant reduction of the processing time of the simulations, allowing the investigation of various geometric configurations. The wave channel has a length of L_T = 320.00 m, a height of H_T = 20.00 m, and the water depth at rest is h = 10.00 m. Furthermore, the submersion of the device is fixed, being H_1 = 3.50 m, and the reservoir dimensions are L_r = 20.00 m and H_r = 6.50 m. The wave flow conditions and dimensions of the reservoir and channel are the same as those used in the work of Martins et al. [24]. Moreover, the magnitude used for H_1 represents the submergence with the best performance found in Martins et al. [24] for the overtopping device without coupled structure. In this sense, it is possible to compare the effect of the seabed trapezoidal obstacle with the case without its use.

Regarding the boundary conditions considered, the generation of waves is caused by the imposition of velocity profiles, defined by the second-order Stokes theory, on the lower-left surface of the computational domain (red line). The atmospheric pressure condition is imposed on the upper-left side and on the upper surface of the channel (blue lines). Meanwhile, on the other surfaces of the channel and on the device, the velocities are prescribed as null, i.e., no-slip and impermeability boundary condition (black lines) is adopted. Furthermore, regarding the initial conditions, the flow is at rest.

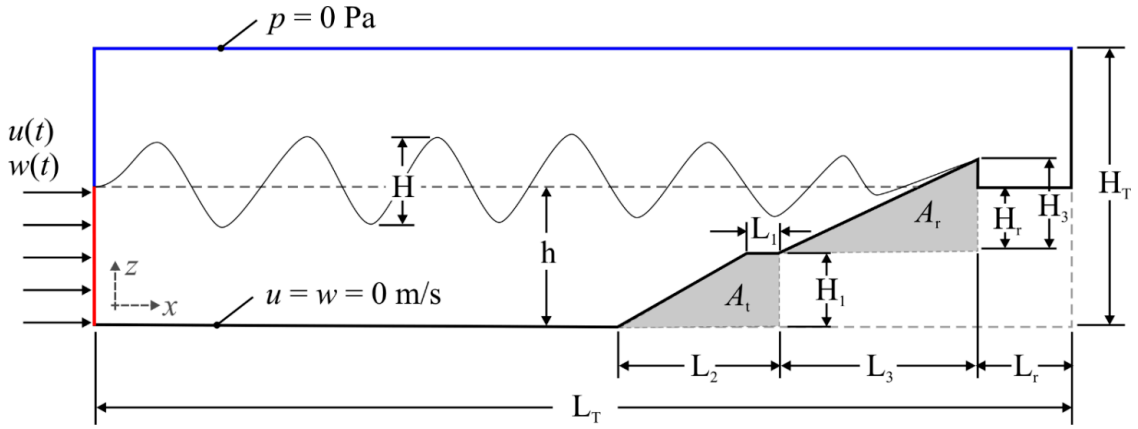

Figure 1. Schematic representation of the two-dimensional computational domain of the overtopping device coupled with the trapezoidal obstacle in the wave channel.

To apply the Constructal Design, defining the performance indicator, constraints, and degrees of freedom is necessary. In the present study, the objective of the flow system, which consists of a wave channel with a coupled converter, is to maximize the amount of water mass that enters the reservoir of the overtopping device.

The problem has three area constraints:

- Total area of the channel (A_T = 6400 m^2),

$$A_T = H_T L_T \tag{16}$$

- Area of the overtopping device ramp (A_r = 78.5 m^2),

$$A_r = \frac{H_3 L_3}{2} \tag{17}$$

- Area of the obstacle placed at the bottom of the channel (A_t = 36.75 m^2):

$$A_t = \frac{(L_1 + L_2) H_1}{2} \tag{18}$$

The constraints A_r and A_t are illustrated in gray in Figure 1. It is possible to rewrite A_r and A_t as fractions areas, using the area of the channel as a reference, respectively, by:

$$\phi_r = \frac{A_r}{A_T} \tag{19}$$

$$\phi_t = \frac{A_t}{A_T} \tag{20}$$

The values of ϕ_r = 0.012 and ϕ_t = 0.006 were fixed.

The defined degrees of freedom are the ratio between the height and length of the ramp of the device (H_3/L_3) and the ratio between the major and minor base of the trapezoidal obstacle (L_1/L_2), which are varied throughout the study. As previously mentioned, the submersion of the device (H_1) is kept fixed, using the best submergence obtained in the work of Martins et al. [24]. Table 2 presents the values investigated for the H_3/L_3 freedom degree and the respective values of H_3 and L_3 adopted in each case.

It is worth noting that the lowest ratio H_3/L_3 = 0.33 was the optimal ratio identified in the study of Martins et al. [24] for the case with H_1 = 3.5 m. On the contrary, the upper limit was established at H_3/L_3 = 0.37, since it was the limit condition where the ramp acts as a WEC and not a breakwater. For each magnitude of H_3/L_3 investigated, 10 different values of the ratio L_1/L_2 were analyzed. Table 3 shows the ratios L_1/L_2 studied and the magnitudes of L_1 and L_2 variables.

Table 2. Values considered for the ratio H_3/L_3.

H_3/L_3	H_3 (m)	L_3 (m)
0.33	7.2300	21.7000
0.34	7.3052	21.4860
0.35	7.4119	21.1768
0.36	7.5170	20.8806
0.37	7.6207	20.5965

Table 3. Values considered for the investigated ratios of L_1/L_2.

L_1/L_2	L_1 (m)	L_2 (m)
0.00	0.00	21.00
0.11	2.08	18.92
0.22	3.79	17.21
0.33	5.21	15.79
0.44	6.42	14.58
0.56	7.54	13.46
0.67	8.43	12.57
0.78	9.20	11.80
0.89	9.89	11.11
1.00	10.50	10.50

The lowest ratio addressed, $L_1/L_2 = 0.00$, represents a triangular obstacle, and the highest ratio, $L_1/L_2 = 1.00$, portrays a rectangular obstacle, while the intermediate ratios, $0.00 < L_1/L_2 < 1.00$, represent trapezoidal obstacles. Figure 2 illustrates different configurations adopted for the obstacle coupled with the overtopping device in extreme and intermediate conditions of the ratio L_1/L_2 and the case without the obstacle: (a) triangular obstacle, (b) trapezoidal obstacle, (c) rectangular obstacle, (d) no obstacle.

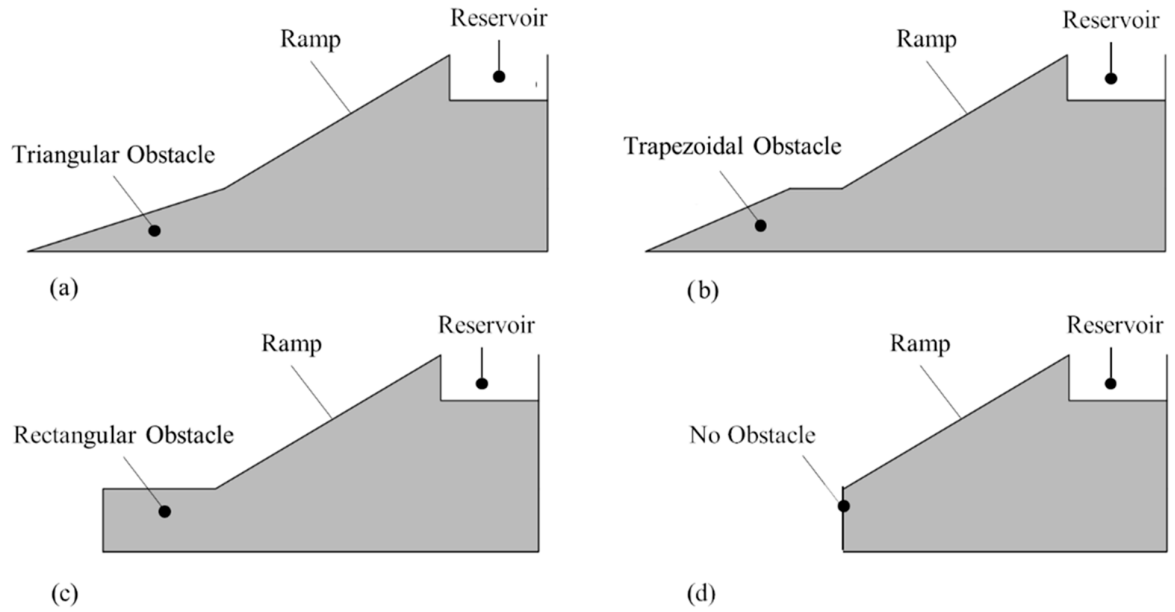

Figure 2. Geometric configurations of the obstacle and case without the obstacle: (**a**) triangular; (**b**) trapezoidal; (**c**) rectangular; and (**d**) no obstacle.

For the geometrical investigation, it is also considered as restriction that $(H_1 + H_3) > (h + H/2)$, thus ensuring that the wave crest does not exceed the maximum height of the device.

The performance indicator in the present study is the total mass of water accumulated in the reservoir, which is determined through:

$$M = \frac{1}{t_f}\int_0^{t_f} \dot{M} dt \tag{21}$$

where t_f refers to the time interval of analysis (s); and $\dot{M}$ is the mass flow rate of water in overtopping occurrences (kg·s^{-1}).

With the constraints, degrees of freedom, and performance indicator defined, it is possible to define the strategy of geometric investigation. The present work uses the association between the Constructal Design and the exhaustive search for geometric optimization. The scheme of investigation can be seen in Figure 3. In the first step, the ratio L_1/L_2 is varied for a constant magnitude of the ratio H_3/L_3. The highest magnitude of the mass of water accumulated in the reservoir is named the once-maximized mass of water accumulated in the reservoir (M_{max}) and the corresponding optimal shape is the once-optimized ratio L_1/L_2, $(L_1/L_2)_o$. In the second step, the same process performed in the first step is repeated for the different magnitudes of the ratio H_3/L_3. The highest magnitude of the mass of water accumulated in the reservoir obtained is called the twice-maximized mass of water accumulated in the reservoir, M_{2max}, and the corresponding optimal configurations are the twice-optimized ratio L_1/L_2, $(L_1/L_2)_{oo}$, and the once-optimized ratio H_3/L_3, $(H_3/L_3)_o$. In the present study, a total of 50 simulations were performed for the geometric investigation.

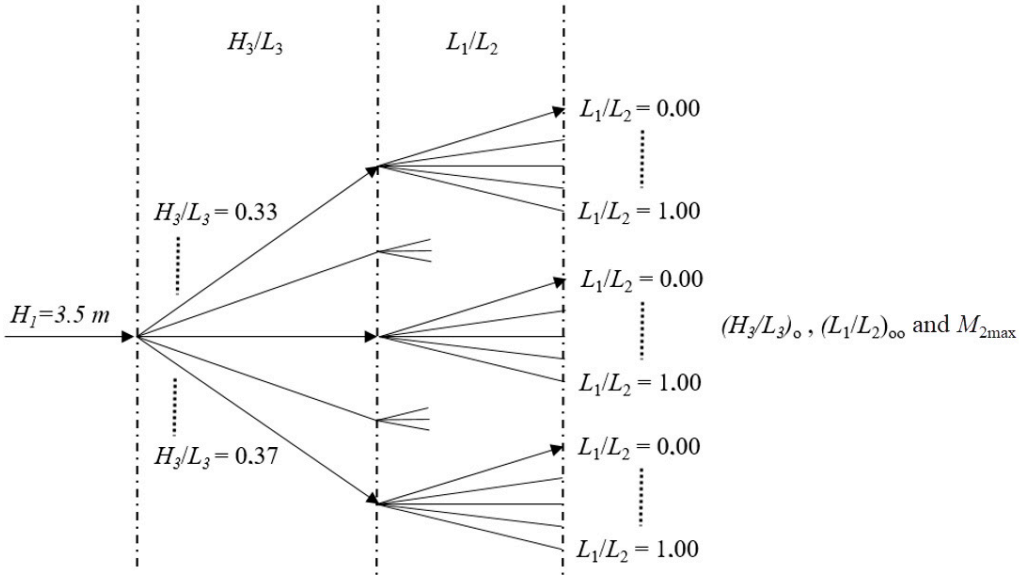

Figure 3. Illustration of the optimization process applied to the overtopping device varying two degrees of freedom.

3. Computational Modeling

For the execution of the present study, numerical simulations of wave generation were carried out in a channel through the software ANSYS Fluent, which is a package of computational fluid dynamics (CFD) based on the Finite Volume Method (FVM) [43]. Such a method consists of dividing the interest domain into several elementary volumes to perform a balance of properties for each finite volume aiming to obtain the corresponding approximate equation and solve one algebraic equations system [43,44].

As for the spatial discretization, a stretched mesh was considered, as in Martins et al. [24]. However, a greater refinement was adopted on both the free surface region, where 30 computational cells per wave height were used, and horizontally, where 70 computational

cells per wavelength were considered, as defined by the mesh independence test. The interaction between the wave flow and the ramp of the overtopping device justifies this greater refinement. Moreover, a greater refinement was employed near the walls due to the more significant gradients of the velocity field in these regions. Figure 4 illustrates the mesh adopted for the computational domain, detailing the region of the overtopping device.

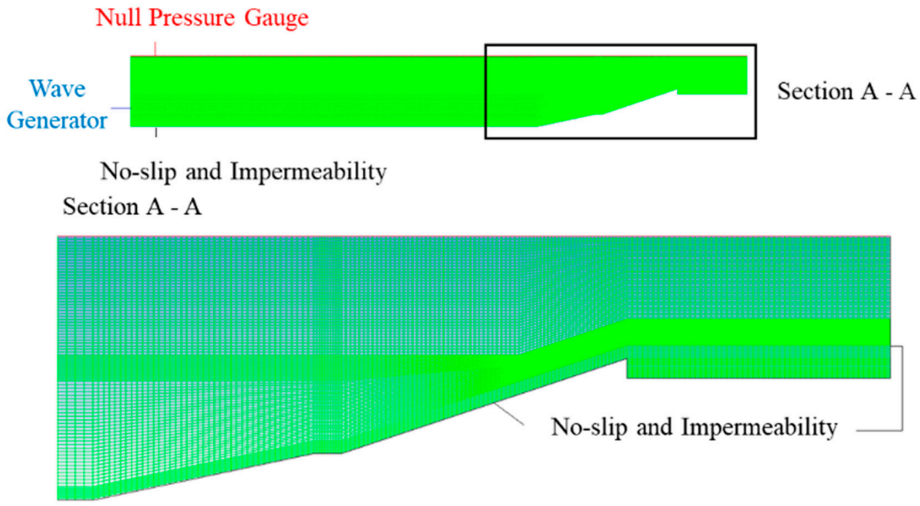

Figure 4. Spatial discretization of overtopping device detailing the regions of ramp and obstacle.

Concerning the numerical procedures used to solve Equations (2)–(5), the methods and parameters used in the present work are presented in Table 4. This numerical methodology is similar to the methodology used in previous studies, as in [23–26]. The computational method has the advantage to allow the simulation of various cases with lower costs than the experimental investigation. However, rigorous investigation of the reliability of the computational method is required to obtain adequate recommendations. This process is performed in the first subsection of the results and discussion section.

Table 4. Methods and parameters used in the present numerical simulations.

Parameters		Numerical Inputs
Solver		Pressure-Based
Pressure-Velocity Coupling		PISO
Spatial Discretization	Gradient Evaluation	Green-Gauss-Cell-Based
	Pressure	PRESTO
	Momentum	First Order Upwind
	Volume Fraction	Geo-Reconstruct [38]
Temporal Differencing Scheme		First Order Implicit
Under-Relaxation Factors	Pressure	0.3
	Momentum	0.7
Residual	Continuity	10^{-6}
	x-velocity	
	z-velocity	
Open Channel Initialization Method		Plane
Regime Flow		Laminar
Time Step (Δt)		2.00×10^{-2} s
Total time of investigation		100 s

4. Results and Discussion

The first results presented refer to studies carried out to determine the spatial and temporal discretization to be adopted and to verify the numerical model used to generate the waves. Then, the results related to the geometric optimization of the obstacle coupled to the overtopping wave energy converter, the main objective of the present study, are presented.

4.1. Mesh and Time Step Independence Study and Verification of the Computational Model

It is worth mentioning that the mesh used was composed of regular rectangles. This kind of finite volume has the advantage of avoiding numerical effects such as false diffusion on the solution of the primary variables of the problem, which could occur by using an irregular mesh with triangular volumes. Thus, in this study, a mesh convergence test was carried out, simulating four cases with a different number of volumes, 19,000, 38,000, 76,000, and 152,000. The results were compared with the calculation of the analytically generated wave (Equation (9)). Therefore, the elevation of the free surface was monitored using a numerical probe of the integral type located at x = 50.00 m.

Furthermore, for the mesh independence test, a time step of $\Delta t = 2.00 \times 10^{-2}$ s was considered. Table 5 shows the MAE average, calculated using Equation (15), and the processing time demanded for each simulation for different meshes investigated.

Table 5. Average MAE and simulation time values for each mesh.

Number of Volumes	MAE (%)	Processing Time (h)
19,000	0.81	5.50
38,000	0.85	8.00
76,000	0.87	12.00
152,000	0.88	19.50

To determine the best mesh, the refinement and processing time of the simulation were considered along with the calculated numerical error. After verifying that the difference between a mesh of 76,000 and one of 152,000 volumes is only 0.01%, lower than the difference observed in the other cases analyzed, a mesh with 76,000 regular rectangular volumes was then adopted.

Since it is a transient problem, the temporal discretization employed was defined by carrying out a time step independence study. For this study, four simulations are performed considering a total time of wave flow over the overtopping device of 100 s and varying the time step by: $\Delta t = 5.00 \times 10^{-3}$ s, $\Delta t = 1.00 \times 10^{-2}$ s, $\Delta t = 2.00 \times 10^{-2}$ s, and $\Delta t = 4.00 \times 10^{-2}$ s.

Table 6 presents the free surface elevation values (η) obtained at x = 50.00 m and for the instant of time t = 15.00 s for each time step studied and the variation among the tested cases. Consequently, the time step of $\Delta t = 2.00 \times 10^{-2}$ s was adopted for the geometric evaluation simulations since it leads to less computational effort among the best time steps. Moreover, only the time step $\Delta t = 2.00 \times 10^{-2}$ s has a higher discrepancy in the magnitude of η compared to the other investigated time steps.

Table 6. Free surface elevation height at x = 50.00 m and t = 15.00 s and the variation among the time steps.

Δt (s)	η (m)	Variation (%)
5.0×10^{-3}	10.507790	-
1.0×10^{-2}	10.507770	1.90×10^{-4}
2.0×10^{-2}	10.507700	6.66×10^{-4}
4.0×10^{-2}	10.496400	1.10×10^{-1}

The analytical solution (Equation (9)) was compared to the numerical solution for a wave generated in a channel without the device to verify the methodology employed. This

comparison is presented in Figure 5, where it is possible to verify that the numerical wave fits well in the analytical solution for $t > 15.00$ s where the stabilization occurred. Before this period, the numerical solution is influenced by the initial condition of inertia of the flow, which is not contemplated in the analytical solution. Thus, the wave generation verification considered the interval of 15.00 s $\leq t \leq$ 80.00 s.

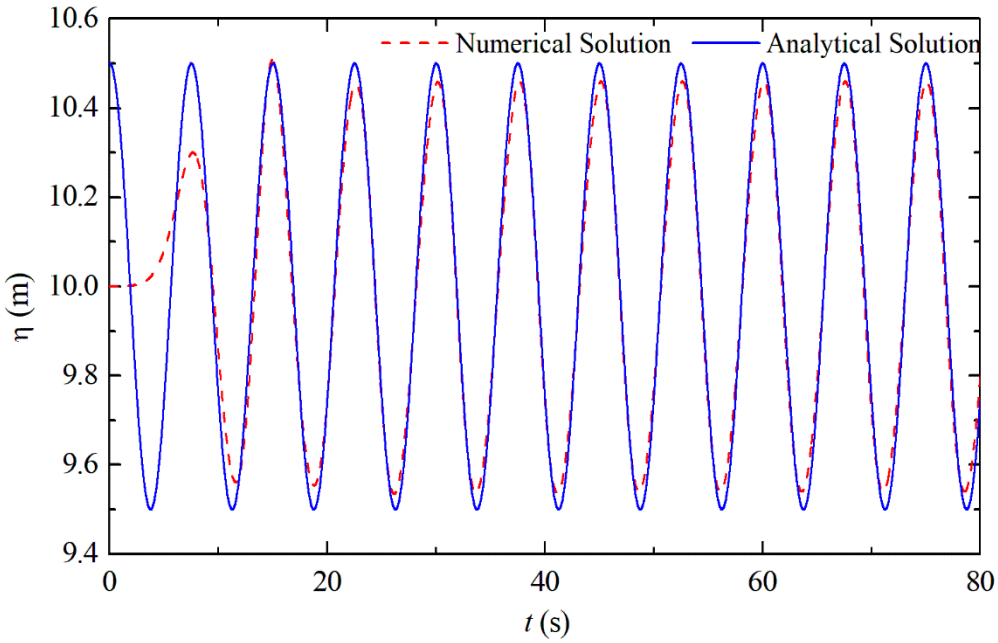

Figure 5. Comparison of the numerical and analytical solution of water surface level in the wave channel.

Evaluating the difference between the analytical and numerical results, when calculating the MAE comparing the elevation of the free surface in the wave channel, considering the depth of h = 10.00 m, a result of approximately 0.10% was obtained. However, when calculating the average MAE considering only the generated wave, i.e., disregarding the water depth on the channel, an average of 8.00% was obtained. Thus, there is a good agreement between the results.

It is also worth mentioning that a validation of the present computational method was performed in a previous research group work. A comparison between the free surface elevation as a function of time in a laboratory-scale wave channel obtained with the present computational model and those obtained experimentally in the work of Goulart [45] was performed. Figure 6 illustrates the wave channel at a laboratory scale used in the work of Goulart [45], which was reproduced numerically with the present computational method. The following dimensions were adopted in the problem: L_T = 34.2 m, H_T = 1.0 m, H_1 = 0.15 m, L_r = 0.5 m, h = 0.862 m, h_1 = 0.392 m, H_3 = 0.279 m, and L_3 = 0.716 m, leading to a ramp angle of 21.3°. Moreover, it is considered that the waves reaching the device have a period of T = 1.94 s, height of H = 0.067 m, and wavelength of λ = 3.54 m. Figure 7 shows the results of the height of water accumulated in the reservoir as a function of time obtained in the experiment of Goulart [45] (red line) and the numerical predictions obtained with the present computational method (black line). As can be observed, the experimental and numerical results were in close agreement, with a difference of 1.8%. The numerical results also predicted the beginning of the overtopping occurrence (t~22.5 s) and the slope of the curve of water accumulation in the reservoir well. Therefore, it is possible to state that the present computational method is verified and validated.

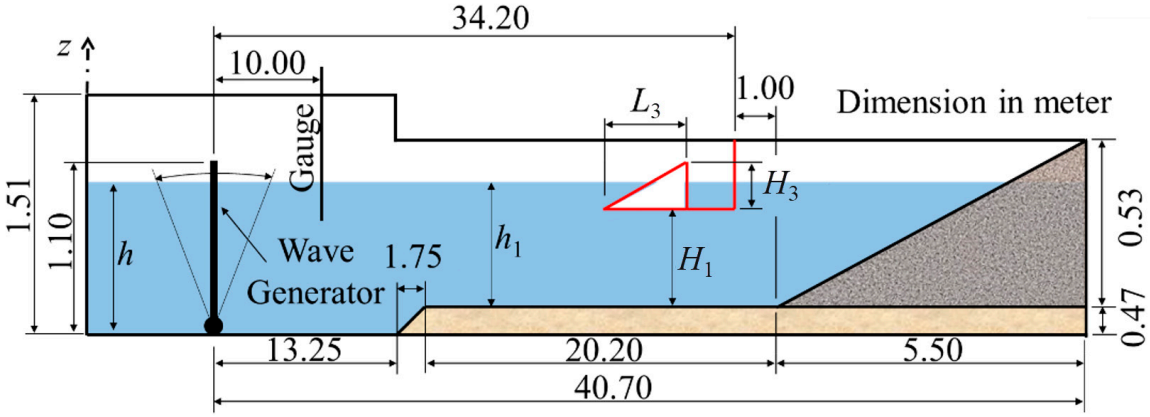

Figure 6. Illustration of the domain investigated experimentally in the work of Goulart [45] and validated with the present computational method.

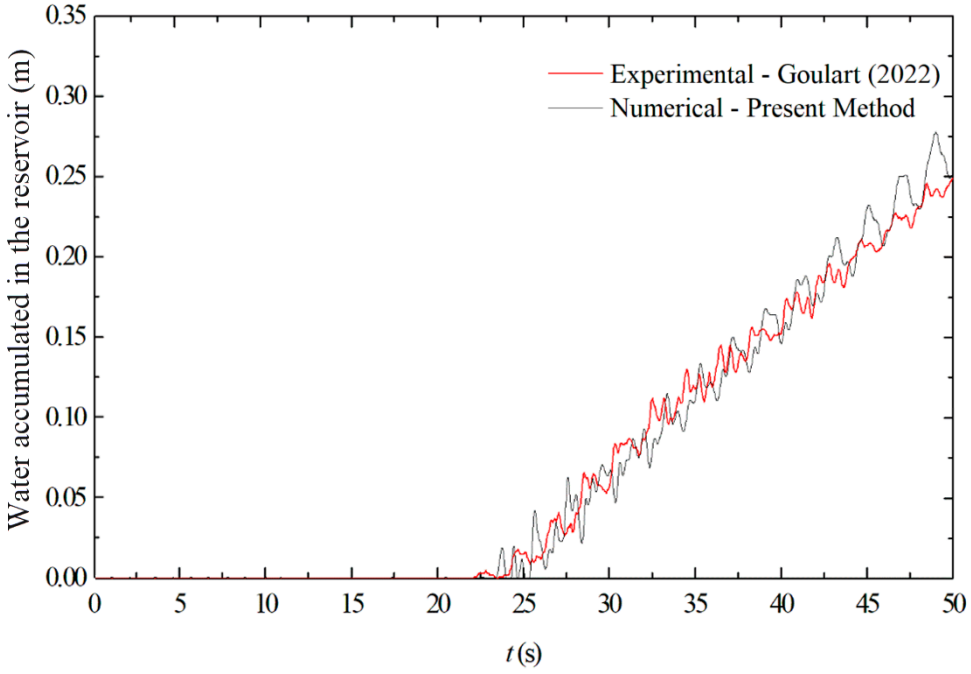

Figure 7. Water accumulated in the reservoir of laboratory-scale overtopping device as function of time obtained experimentally in Goulart [45] and with the present numerical method.

4.2. Geometric Investigation of the Overtopping Device with Coupled Obstacle

To perform the geometric evaluation, the geometry of the overtopping device with five different H_3/L_3 ratios, previously studied in [24], is considered. The obstacle attached to the device varied between the lowest magnitude of $L_1/L_2 = 0.00$, representing a triangular configuration, and the highest magnitude of $L_1/L_2 = 1.00$, representing a rectangular configuration. Intermediate ratios of L_1/L_2 ($0.00 < L_1/L_2 < 1.00$) refer to trapezoidal obstacles. The total sum of the mass of water entering the reservoir over the 100.00 s simulated was calculated to compare the performance of the different geometries.

Figure 8 shows the effect of the ratio L_1/L_2 over the total amount of water mass accumulated in the reservoir over the time interval considered (M) for different values of H_3/L_3. It is possible to observe that the ratio $H_3/L_3 = 0.33$ conducted to the maximum water accumulation in the reservoir was almost $M = 40{,}000$ kg, while ratios of $H_3/L_3 = 0.37$ led to an amount of mass in the range of $M = 10{,}000$ kg, i.e., a ratio of 4.5 times between the best and worst conditions of H_3/L_3. Results also indicated that the effect of L_1/L_2 on the device performance was significantly lower than the effect of H_3/L_3 over M, i.e., the sensibility of

H_3/L_3 was much higher than L_1/L_2 over the overtopping performance. One example can be noticed for H_3/L_3 = 0.33, where the difference between the best configuration of L_1/L_2, $(L_1/L_2)_o$ = 0.67 led to a performance of only 5.00% superiority to that achieved for the worst configuration (L_1/L_2 = 0.11). As the magnitude of the ratio H_3/L_3 increases, the influence of the ratio L_1/L_2 over m increases, as can be attested for the ratio H_3/L_3 = 0.37, where the best configuration of L_1/L_2, $(L_1/L_2)_o$ = 0.67 conducted a performance nearly 20.00% superior than the triangular configuration (L_1/L_2 = 0.00) which conducted to the worst performance. Moreover, for all cases using H_3/L_3 an optimal intermediate configuration of L_1/L_2 is obtained. Despite presenting a secondary contribution, the ratio L_1/L_2 improved the overtopping device, mainly for non-optimized ratios of H_3/L_3.

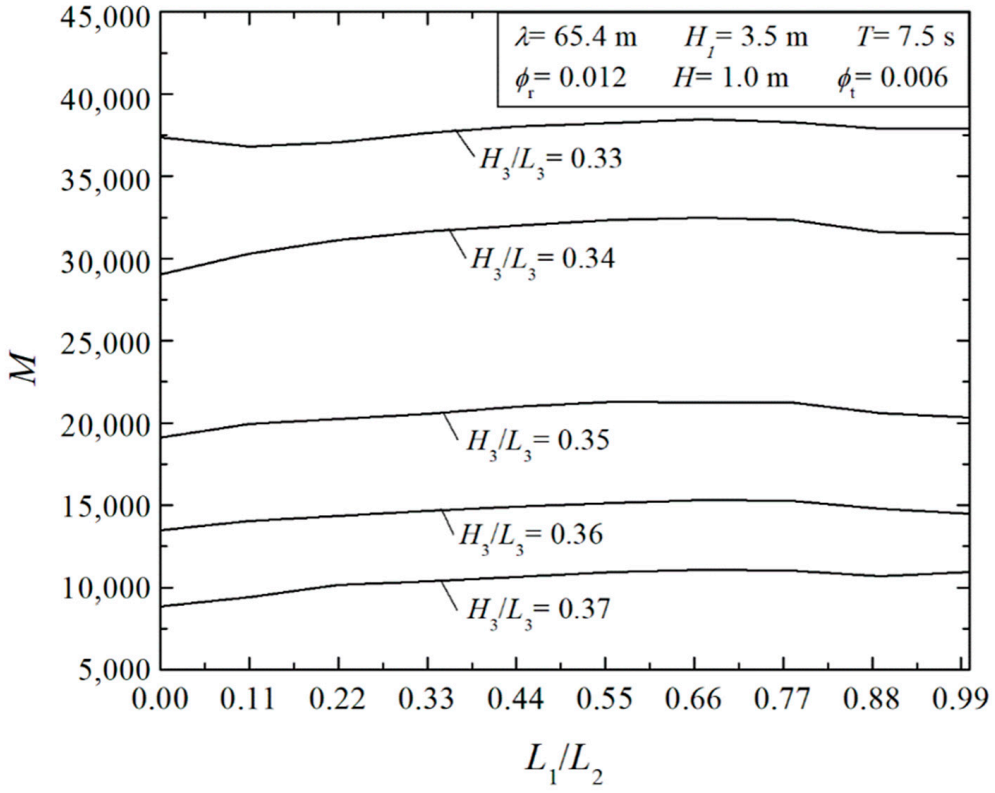

Figure 8. Influence of ratio L_1/L_2 over the mass of water considering different H_3/L_3 values.

The best configurations found in Figure 8 are summarized in Figure 9, presenting the effect of the ratio H_3/L_3 over the once-maximized mass of water accumulated in the reservoir, M_{max}. The results reinforced the strong sensitivity of the ratio H_3/L_3 over the overtopping device performance. It is also noticed that, for almost all cases, the ratio L_1/L_2 = 0.67 led to the best performance, except for the case with H_3/L_3 = 0.35, where the ratio L_1/L_2 = 0.54 was the best. Thus, the L_1/L_2 ratio that provides the best performance in all cases has a trapezoidal shape. When considering a triangular obstacle, L_1/L_2 = 0.00, the wave flow suffers a dispersion and the overtopping is not favorable, i.e., the configuration of the ramp and obstacle acts as a beach, smoothing the intensity of the wave that reaches the final stage of the ramp. On the other hand, considering a rectangular obstacle, L_1/L_2 = 1.00, there is a greater reflection of the wave, also disfavoring the intensity of the flow that reaches the ramp.

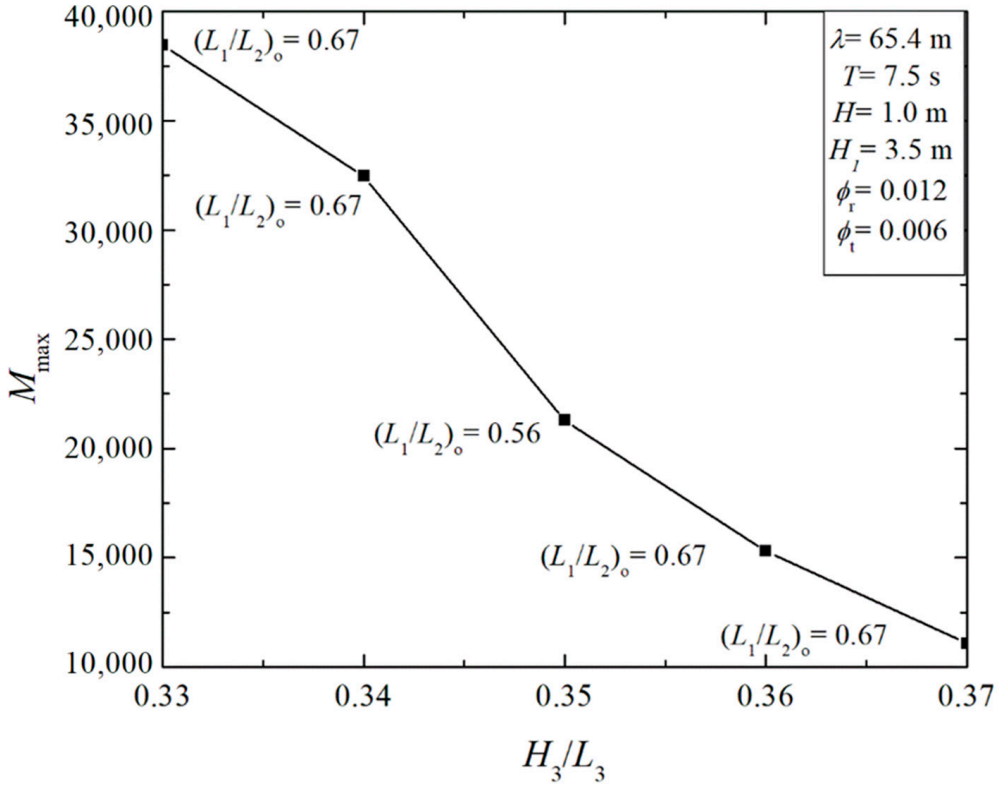

Figure 9. Influence of ratio H_3/L_3 over once-maximized mass of water and corresponding optimal ratios of L_1/L_2.

The fluid dynamic behavior of the problem is shown, for some instances of time, in Figures 10 and 11, where the water volumetric fraction and velocity fields are displayed. Thereby, it is possible to observe how the wave flows over the device for the case with the optimal ratio of $(H_3/L_3)_o = 0.33$, considering three different obstacle ratios, (a) $L_1/L_2 = 0.11$, (b) $(L_1/L_2)_{oo} = 0.67$, and (c) $L_1/L_2 = 1.00$. Furthermore, in Figure 10, water is represented by red, while air is represented by blue. Through the volume fraction fields in Figure 10, it is possible to observe the overtopping occurrence in the instances of time t = 74.00 s and 75.00 s for different configurations of L_1/L_2 investigated. In all plotted cases, between the time instances of 73.00 s $\leq t \leq$ 75.00 s, it is observed that the water mass generates a high inflection in the free surface, which leads to a wave-breaking process, causing the overtopping. From t = 76.00 s on, it is noted that the wave stabilizes and the mass of water begins to move in the opposite direction, towards the base of the ramp. In Figure 11, among the color scales, red represents higher velocities while blue represents the lower ones. In all situations, it is observed that the highest magnitudes occur in the air due to the lower air density. In the time interval 74.00 s $\leq t \leq$ 75.00 s, the mass of water entering the reservoir causes a boundary layer detachment, increasing the magnitude of velocity fields even more in the airflow near the water jet entering the reservoir. In the water region, the highest magnitudes can be noticed when the wave is in the imminence to overtop the ramp and after the overtopping, when the water is in the opposite direction of the wave flow. In this situation, the water going down the ramp meets the next incident wave, generating a mixture of streams and intensifying the velocity magnitude. Concerning the comparison of ratios L_1/L_2, only slight differences are observed in the volume fraction and velocity fields, which are reflected in the small differences found between the best and worst configurations.

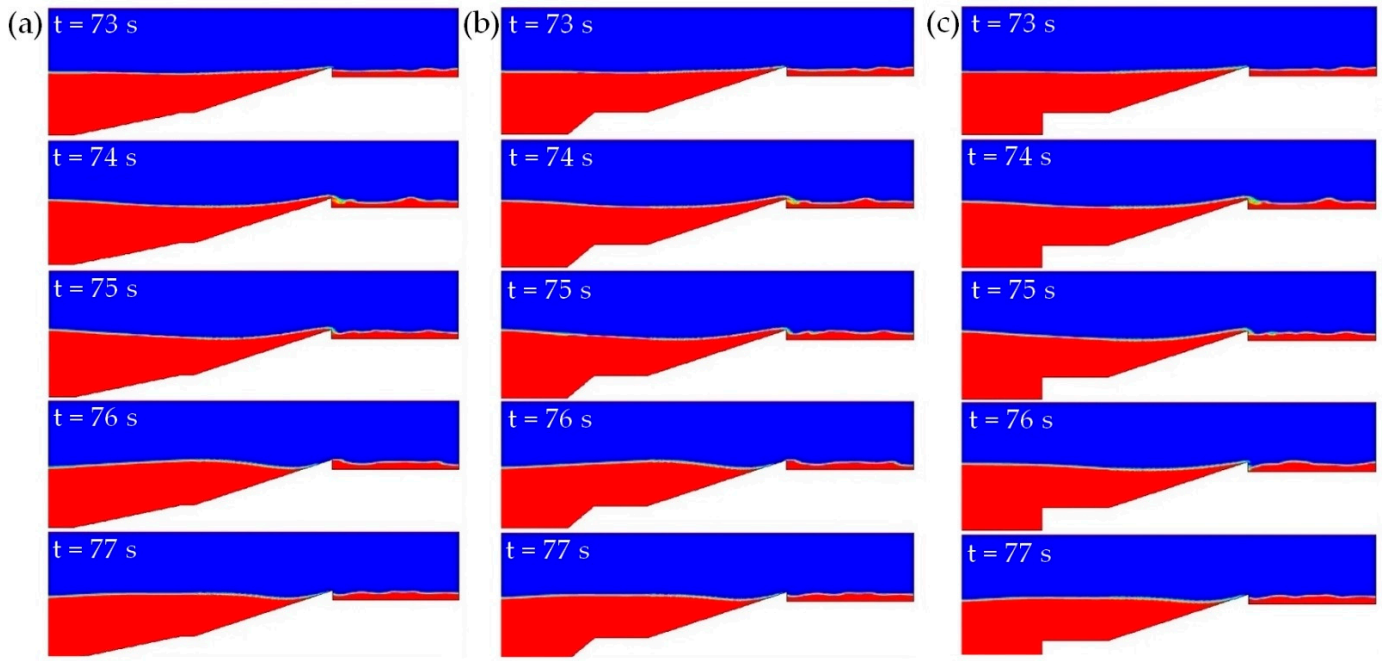

Figure 10. Transient fields of volume fraction for $(H_3/L_3)_o$ = 0.33 and the ratios: (**a**) L_1/L_2 = 0.11; (**b**) $(L_1/L_2)_o$ = 0.67; and (**c**) L_1/L_2 = 1.00.

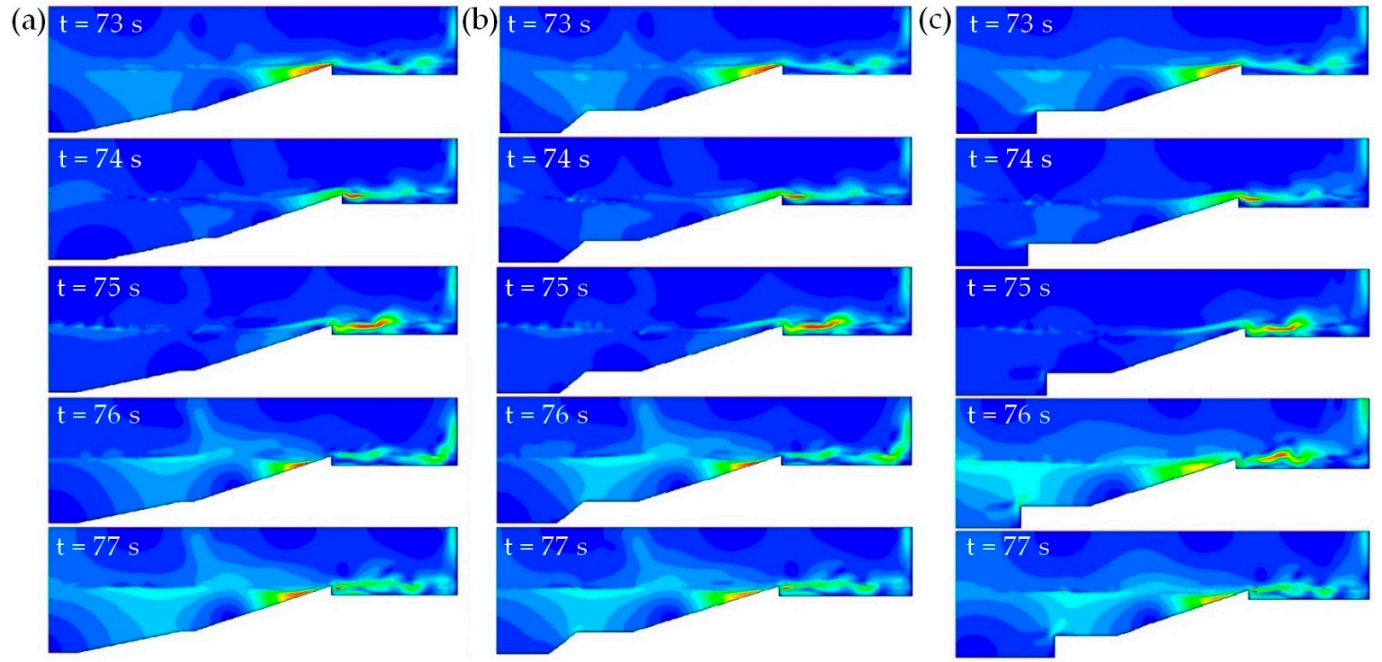

Figure 11. Transient fields of velocity fields for $(H_3/L_3)_o$ = 0.33 and the ratios: (**a**) L_1/L_2 = 0.11; (**b**) $(L_1/L_2)_o$ = 0.67; and (**c**) L_1/L_2 = 1.00.

Finally, a comparison among three different configurations coupled with the overtopping device was performed: 1—trapezoidal for the optimal ratio of L_1/L_2, 2—rectangular (L_1/L_2 = 1.00), 3—triangular (L_1/L_2 = 0.00), and one configuration without a seabed structure (for the same conditions studied in the work of Martins et al. [25]). Figure 12 illustrates the effect of the ratio H_3/L_3 over the amount of mass overtopped in the reservoir (M) along the time interval for the four studied configurations. It is important to mention that the mass accumulated in the reservoir is directly proportional to the potential energy of water

in the device, considering the use of the same reservoir for all investigated configurations, as is the case here. Therefore, the highest magnitudes of M led to the highest energy conversion when the water in the reservoir is expanded in a low-head turbine. Results demonstrated that the best configuration is the trapezoidal, followed by the rectangular and triangular configurations, respectively, regardless of the ratio H_3/L_3. Moreover, results demonstrated that the differences between the different configurations with the coupled structure are not significant, mainly for $(H_3/L_3)_o = 0.33$, where differences are nearly 4%. Despite the influence of the degree of freedom of L_1/L_2 being smaller than that of H_3/L_3, analyzing the results shown in Figure 12, it is possible to state that the configuration of the obstacle-ramp set captures a greater amount of water mass in the reservoir, making this configuration more efficient compared to the conventional overtopping device. For the twice optimal configuration, i.e., for $(H_3/L_3)_o = 0.33$ and $(L_1/L_2)_{oo} = 0.67$, the coupling of the trapezoidal structure improved the device performance by 30% when compared to the conventional device for the same H_3/L_3 ratio. For non-optimized ratios of H_3/L_3, the influence of the seabed structure is even more important. For instance, for $H_3/L_3 = 0.34$, the performance reached with the trapezoidal structure is around 1.7 times superior to the case without the structure.

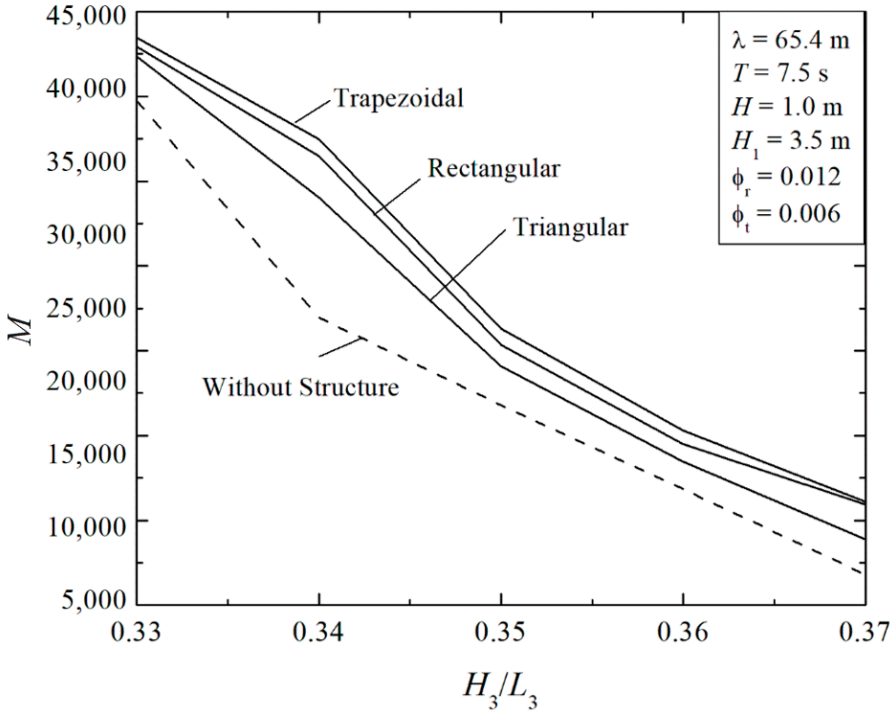

Figure 12. Comparison between the performance of the device without an obstacle studied in [25] with the device integrated with different geometric shapes of obstacles.

5. Conclusions

In the present paper, a numerical analysis and optimization study was carried out to evaluate the geometry of a seabed structure coupled with the ramp of an onshore overtopping device. The geometry was varied to maximize the amount of water from the incident waves entering the reservoir of the overtopping device. The variation of two degrees of freedom was analyzed, along with the ratio between the major and minor base of the trapezoidal obstacle (L_1/L_2) and the ratio between the height and length of the device ramp (H_3/L_3). The geometric evaluation was performed using the Constructal Design method, and the optimization was performed using the exhaustive search method.

In all cases analyzed, the maximum amount of water that entered the reservoir over time occurred for the lowest ratio of (H_3/L_3), $(H_3/L_3)_o = 0.33$, associated with intermediate geometries of L_1/L_2, i.e., trapezoidal configurations. With the exception of the ratio

H_3/L_3 = 0.35, the best ratios of L_1/L_2 were obtained for $(L_1/L_2)_o$ = 0.67. On the contrary, the worst performances were achieved for the highest magnitudes of H_3/L_3 and lower magnitudes of L_1/L_2. It is important to note that the H_3/L_3 ratio had a bigger influence on the device performance than the L_1/L_2 ratio had over the device performance. Despite that, the L_1/L_2 ratio led to improvements of approximately 4% and 20% when comparing the best and worst geometry ratios of H_3/L_3.

Results, in general, showed the applicability and efficiency of the Constructal Design in the geometric evaluation after finding that the best geometry has a performance four times higher than the case in which the worst geometry was adopted for the obstacle-ramp set. Finally, the comparative numerical analysis between an overtopping device without an obstacle and a device with a coupled structure proved that the use of the obstacle provides better performance for the wave energy converter than a conventional device. For the ratio $(H_3/L_3)_o$ = 0.33, the use of the coupled structure improved the performance by 30% in comparison with the case without a structure studied in the work of Martins et al. [25].

For future studies, it is suggested to vary both the construction area of the ramp and the coupled structure, as well as to analyze the variation of the submersion of the device. Still, it is suggested that optimization studies of wave energy converter devices be carried out using the WaveMIMO methodology, which allows the numerical simulation of irregular waves based on realistic sea states. In this way, it is possible to optimize an overtopping device considering the wave climate of the place where it is to be installed.

Author Contributions: Conceptualization, A.S.d.B., L.A.O.R., B.N.M., L.A.I., M.d.N.G. and E.D.d.S.; methodology, A.S.d.B., M.d.S.P., B.N.M., L.A.I., M.d.N.G. and E.D.d.S.; software, A.S.d.B., B.N.M., L.A.I., M.d.N.G. and E.D.d.S.; validation, A.S.d.B., M.d.S.P., B.N.M., M.d.N.G. and E.D.d.S.; formal analysis, C.F., L.A.O.R., B.N.M., L.A.I., M.d.N.G. and E.D.d.S.; investigation, A.S.d.B., M.d.S.P., B.N.M., L.A.I. and E.D.d.S.; resources, C.F., L.A.O.R., L.A.I. and E.D.d.S.; data curation, B.N.M., L.A.I., M.d.N.G. and E.D.d.S.; writing—original draft preparation, M.d.S.P., B.N.M. and E.D.d.S.; writing—review and editing, C.F., L.A.O.R., L.A.I. and M.d.N.G.; visualization, C.F., L.A.O.R., L.A.I. and E.D.d.S.; supervision, M.d.N.G., B.N.M. and E.D.d.S.; project administration, L.A.O.R., B.N.M., L.A.I., M.d.N.G. and E.D.d.S.; funding acquisition, C.F., L.A.O.R., L.A.I., M.d.N.G. and E.D.d.S. All authors have read and agreed to the published version of the manuscript.

Funding: This research was funded by Brazilian Coordination for the Improvement of Higher Education Personnel—CAPES (Finance Code 001), Research Support Foundation of the State of Rio Grande do Sul—FAPERGS (Public Call FAPERGS 07/2021—*Programa Pesquisador Gaúcho*—PqG—21/2551-0002231-0), Brazilian National Council for Scientific and Technological Development—CNPq (Processes: 309648/2021-1, 307791/2019-0, 308396/2021-9, 440010/2019-5, and 440020/2019-0), and Ministry of Science, Technology, Innovation and Communications (Public Call MCTIC/CNPq N°28/2018—Universal).

Institutional Review Board Statement: Not applicable.

Informed Consent Statement: Not applicable.

Data Availability Statement: The data presented in this study are available on request from the corresponding author. The data are not publicly available due to privacy reasons.

Acknowledgments: The authors thank FAPERGS (Public Call FAPERGS 07/2021—*Programa Pesquisador Gaúcho*—PqG—process: 21/2551-0002231-0) and CNPq (Public Call CNPQ/EQUINOR *Energia Ltd.a* N° 38/2018—Processes: 440010/2019-5 and 440020/2019-0) for the financial support. The authors A.S.d.B. and M.d.S.P. thank CAPES (Finance Code 001) for their master's scholarship. The author M.d.N.G. thanks MCTIC (Public Call MCTIC/CNPq N° 28/2018—Universal). The authors L.A.O.R., L.A.I. and E.D.d.S. are grant holders of the CNPq (processes: 307791/2019-0, 309648/2021-1, and 308396/2021-9, respectively).

Conflicts of Interest: The authors declare no conflict of interest. The funders had no role in the design of the study, in the collection, analyses, or interpretation of data, or in the writing of the manuscript, as well as in the decision to publish the results.

Nomenclature

A_T	channel total area [m^2]
A_t	trapezoidal obstacle area [m^2]
A_r	overtopping device ramp area [m^2]
c	wave celerity [m/s]
$\vec{g}$	gravity acceleration vector [m/s^2]
H	wave height [m]
h	water depth [m]
H_r	reservoir height [m]
H_T	wave channel height [m]
H_1	device submersion [m]
h_1	water depth in experimental test [m]
H_3	ramp height [m]
i	counter variable [-]
k	wave number [m^{-1}]
L_r	reservoir length [m]
L_T	wave channel length [m]
L_1	minor base of the trapezoidal obstacle [m]
L_2	major base of the trapezoidal obstacle [m]
L_3	ramp length [m]
M	water mass accumulated [kg]
$\dot{M}$	mass flow rate [$kg{\cdot}s^{-1}$]
N	total number of data [-]
O	numerical data [m]
P	analytical data [m]
p	static pressure [Pa]
T	wave period [s]
t	time [s]
t_f	time interval of analysis [s]
u	horizontal velocity component [m/s]
$\vec{v}$	velocity vector [m/s]
x	horizontal coordinate axis [m]
w	vertical velocity component [m/s]
z	vertical coordinate axis [m]
α	volume fraction [-]
η	water-free surface elevation [m]
λ	wavelength [m]
μ	dynamic viscosity [kg/(m.s)]
ρ	fluid density [kg/m^3]
$\overline{\overline{\tau}}$	strain rate tensor [N/m^2]
ϕ_r	fraction area of the ramp [-]
ϕ_t	fraction area of the trapezoidal obstacle [-]
φ	velocity potential [m^2/s]
ω	angular wave frequency [Hz]

References

1. Østergaard, P.A.; Duic, N.; Noorollahi, Y.; Kalogirou, S. Renewable energy for sustainable development. *Renew. Energy* **2022**, *199*, 1145–1152. [CrossRef]
2. Hernández-Fontes, J.V.; Martínez, M.L.; Wojtarowski, A.; González-Mendoza, J.L.; Landgrave, R.; Silva, R. Is ocean energy an alternative in developing regions? A case study in Michoacan, Mexico. *J. Clean. Prod.* **2020**, *266*, 121984. [CrossRef]
3. Clemente, D.; Rosa-Santos, P.; Taveira-Pinto, F. On the potential synergies and applications of wave energy converters: A review. *Renew. Sustain. Energy Rev.* **2021**, *135*, 110162. [CrossRef]
4. Liu, Z.; Shi, H.; Cui, Y.; Kim, K. Experimental study on overtopping performance of a circular ramp wave energy converter. *Renew. Energy* **2017**, *104*, 163–176. [CrossRef]
5. Liu, Z.; Han, Z.; Shi, H.; Yang, W. Experimental study on multi-level overtopping wave energy convertor under regular waves conditions. *Int. J. Nav. Archit. Ocean. Eng.* **2018**, *10*, 651–659. [CrossRef]

6. Rosa-Santos, P.; Taveira-Pinto, F.; Clemente, D.; Cabral, T.; Fiorentin, F.; Belga, F.; Morais, T. Experimental Study of a Hybrid Wave Energy Converter Integrated in a Harbor Breakwater. *J. Mar. Sci. Eng.* **2019**, *7*, 33. [CrossRef]
7. Peng, W.; Zhang, Y.; Yang, X.; Zhang, J.; He, R.; Liu, Y.; Chen, R. Hydrodynamic Performance of a Hybrid System Combining a Fixed Breakwater and a Wave Energy Converter: An Experimental Study. *Energies* **2020**, *13*, 5740. [CrossRef]
8. Singh, U.; Abdussamie, N.; Hore, J. Hydrodynamic performance of a floating offshore OWC wave energy converter: An experimental study. *Renew. Sustain. Energy Rev.* **2020**, *117*, 109501. [CrossRef]
9. Clemente, D.; Calheiros-Cabral, T.; Rosa-Santos, P.; Taveira-Pinto, F. Hydraulic and Structural Assessment of a Rubble-Mound Breakwater with a Hybrid Wave Energy Converter. *J. Mar. Sci. Eng.* **2021**, *9*, 922. [CrossRef]
10. Liu, Z.; Xu, C.; Kim, K. Overall performance of a model OWC system under the free-spinning mode: An experimental study. *Ocean. Eng.* **2021**, *227*, 108890. [CrossRef]
11. Shahroozi, Z.; Göteman, M.; Engström, J. Experimental investigation of a point-absorber wave energy converter response in different wave-type representations of extreme sea states. *Ocean. Eng.* **2022**, *248*, 110693. [CrossRef]
12. Pecher, A.; Kofoed, J.P. *Handbook of Ocean Wave Energy*; Springer Open: Cham, Switzerland, 2017.
13. Seibt, F.M.; Camargo, F.V.; Dos Santos, E.D.; Neves, G.M.; Rocha, L.A.O.; Isoldi, L.A.; Fragassa, C. Numerical evaluation on the efficiency of the submerged horizontal plate type wave energy converter. *FME Trans.* **2019**, *47*, 543–551. [CrossRef]
14. Carmigniani, R.; Leroy, A.; Violeau, D. A simple SPH model of a free surface water wave pump: Waves above a submerged plate. *Coast. Eng. J.* **2019**, *61*, 96–108. [CrossRef]
15. He, M.; Gao, X.; Xu, W.; Ren, B.; Wang, H. Potential application of submerged horizontal plate as a wave energy breakwater: A 2D study using the WCSPH method. *Ocean. Eng.* **2019**, *185*, 27–46. [CrossRef]
16. Kofoed, J.P.; Frigaard, P.; Friis-Madsen, E.; Sørensen, H.C. Prototype testing of the wave energy converter wave dragon. *Renew. Energy* **2006**, *31*, 181–189. [CrossRef]
17. Han, Z.; Liu, Z.; Shi, H. Numerical study on overtopping performance of a multi-level breakwater for wave energy conversion. *Ocean. Eng.* **2018**, *150*, 94–101. [CrossRef]
18. Lauro, E.D.; Maza, M.; Lara, J.L.; Losada, I.J.; Vicinanza, D. Advantages of an innovative vertical breakwater with an overtopping wave energy converter. *Coast. Eng.* **2020**, *159*, 103713. [CrossRef]
19. Contestabile, P.; Crispino, G.; Russo, S.; Gisonni, C.; Cascetta, F.; Vicinanza, D. Crown wall modifications as response to wave overtopping under a future sea level scenario: An experimental parametric study for an innovative composite seawall. *Appl. Sci.* **2020**, *10*, 2227. [CrossRef]
20. Contestabile, P.; Russo, S.; Azzellino, A.; Cascetta, F.; Vicinanza, D. Combination of local sea winds/land breezes and nearshore wave energy resource: Case study at MaRELab (Naples, Italy). *Energy Convers. Manag.* **2022**, *257*, 115356. [CrossRef]
21. Bejan, A. *Shape and Structure, from Engineering to Nature*; Cambridge University Press: Cambridge, UK, 2000.
22. Dos Santos, E.D.; Machado, B.N.; Zanella, M.M.; Gomes, M.; Das, N.; Souza, J.A.; Isoldi, L.A.; Rocha, L.A.O. Numerical Study of the Effect of the Relative Depth on the Overtopping Wave Energy Converters According to Constructal Design. *Defect Diffus. Forum* **2014**, *348*, 232–244. [CrossRef]
23. Goulart, M.M.; Martins, J.C.; Acunha Junior, I.C.; das Neves Gomes, M.; Souza, J.A.; Rocha, L.A.O.; Isoldi, L.A.; dos Santos, E.D. Constructal design of an onshore overtopping device in real scale for two different depths. *Mar. Syst. Ocean. Technol.* **2015**, *10*, 120–129. [CrossRef]
24. Martins, J.C.; Goulart, M.M.; Gomes, M.N.; Souza, J.A.; Rocha, L.A.O.; Isoldi, L.A.; Santos, E.D. Geometric evaluation of the main operational principle of an overtopping wave energy converter by means of Constructal Design. *Renew. Energy* **2018**, *118*, 727–741. [CrossRef]
25. Martins, J.C.; Fragassa, C.; Goulart, M.M.; dos Santos, E.D.; Isoldi, L.A.; das Neves Gomes, M.; Rocha, L.A.O. Constructal Design of an Overtopping Wave Energy Converter Incorporated in a Breakwater. *J. Mar. Sci. Eng.* **2022**, *10*, 471. [CrossRef]
26. Gomes, M.; Das, N.; Lorenzini, G.; Rocha, L.A.O.; Dos Santos, E.D.; Isoldi, L.A. Constructal Design Applied to the Geometric Evaluation of an Oscillating Water Column Wave Energy Converter Considering Different Real Scale Wave Periods. *J. Eng. Thermophys.* **2018**, *27*, 173–190. [CrossRef]
27. Gomes, M.N.; De Deus, M.J.; Dos Santos, E.D.; Isoldi, L.A.; Rocha, L.A.O. Analysis of the Geometric Constraints Employed in Constructal Design for Oscillating Water Column Devices Submitted to the Wave Spectrum Through a Numerical Approach. *Defect Diffus. Forum* **2019**, *390*, 193–210. [CrossRef]
28. Bejan, A. *The Physics of Life: The Evolution of Everything*; St. Martin's Press: New York, NY, USA, 2016.
29. Bejan, A.; Lorente, S. *Design with Constructal Theory*; Wiley: New Jersey, NJ, USA, 2008.
30. Bejan, A.; Zane, J. *Design in Nature*; Doubleday: New York, NY, USA, 2012.
31. Bejan, A.; Lorente, S. Constructal Theory of generation of configuration in nature and engineering. *J. Appl. Phys.* **2006**, *100*, 5. [CrossRef]
32. Guimarães, R.C.; Oleinik, P.H.; Kirinus, E.P.; Lopes, B.V.; Trombetta, T.B.; Marques, W.C. An overview of the Brazilian continental shelf wave energy potential. *Reg. Stud. Mar. Sci.* **2018**, *25*, 100446. [CrossRef]
33. Oleinik, P.H.; Marques, W.C.; Kirinus, E.P. Evaluation of the seasonal pattern of wind-driven waves on the south-southeastern Brazilian shelf. *Defect Diffus. Forum* **2017**, *370*, 141–151. [CrossRef]

34. Machado, B.N.; Oleinik, P.H.; Kirinus, E.P.; Dos Santos, E.D.; Rocha, L.A.O.; Gomes, M.; Das, N.; Conde, J.M.P.; Isoldi, L.A. WaveMIMO Methodology: Numerical Wave Generation of a Realistic Sea State. *J. Appl. Comput. Mech.* **2021**, *1*, 2129–2148. [CrossRef]
35. Maciel, R.P.; Fragassa, C.; Machado, B.N.; Rocha, L.A.O.; Dos Santos, E.D.; Gomes, M.; Das, N.; Isoldi, L.A. Verification and Validation of a Methodology to Numerically Generate Waves Using Transient Discrete Data as Prescribed Velocity Boundary Condition. *J. Mar. Sci. Eng.* **2021**, *9*, 896. [CrossRef]
36. Hubner, R.G.; Fragassa, C.; Paiva, M.S.; Oleinik, P.H.; Gomes, M.N.; Rocha, L.A.O.; Santos, E.D.; Machado, B.N.; Isoldi, L.A. Numerical Analysis of an Overtopping Wave Energy Converter Subjected to the Incidence of Irregular and Regular Waves from Realistic Sea States. *J. Mar. Sci. Eng.* **2022**, *10*, 1084. [CrossRef]
37. Jiao, P.; Matin Nazar, A.; Egbe, K.-J.I.; Barri, K.; Alavi, A.H. Magnetic capsulate triboelectric nanogenerators. *Sci. Rep.* **2022**, *12*, 89. [CrossRef] [PubMed]
38. Hirt, C.W.; Nichols, B.D. Volume of fluid (VOF) method for the dynamics of free boundaries. *J. Comput. Phys.* **1981**, *39*, 201–225. [CrossRef]
39. Schlichting, H. *Boundary Layer Theory*; McGraw-Hill: New York, NY, USA, 1979.
40. Chakrabarti, S.K. *Handbook of Offshore Engineering*; Elsevier: St. Louis, PH, USA, 2005.
41. Michael, E.; McCormick, M.E. *Ocean Engineering Mechanics with Applications*; Cambridge University Press: New York, NY, USA, 2009.
42. Chai, T.; Draxler, R.R. Root mean square error (RMSE) or mean absolute error (MAE)? Arguments against avoiding RMSE in the literature. *Geosci. Model Dev.* **2014**, *7*, 1247–1250. [CrossRef]
43. Versteeg, H.K.; Malalasekera, W. *An Introduction to Computational Fluid Dynamics—The Finite Volume Method*; Pearson Education Limited: London, UK, 2007.
44. Patankar, S.V. *Numerical Heat Transfer and Fluid Flow*; McGraw-Hill: New York, NY, USA, 1980.
45. Goulart, M.M. Validation of a Numerical Model of an Overtopping Device and Numerical and Experimental Research of Geometry Applying the Constructal Design Method. Master's Thesis, Universidade Federal do Rio Grande, Rio Grande, Brazil, 2022. (In Portuguese)